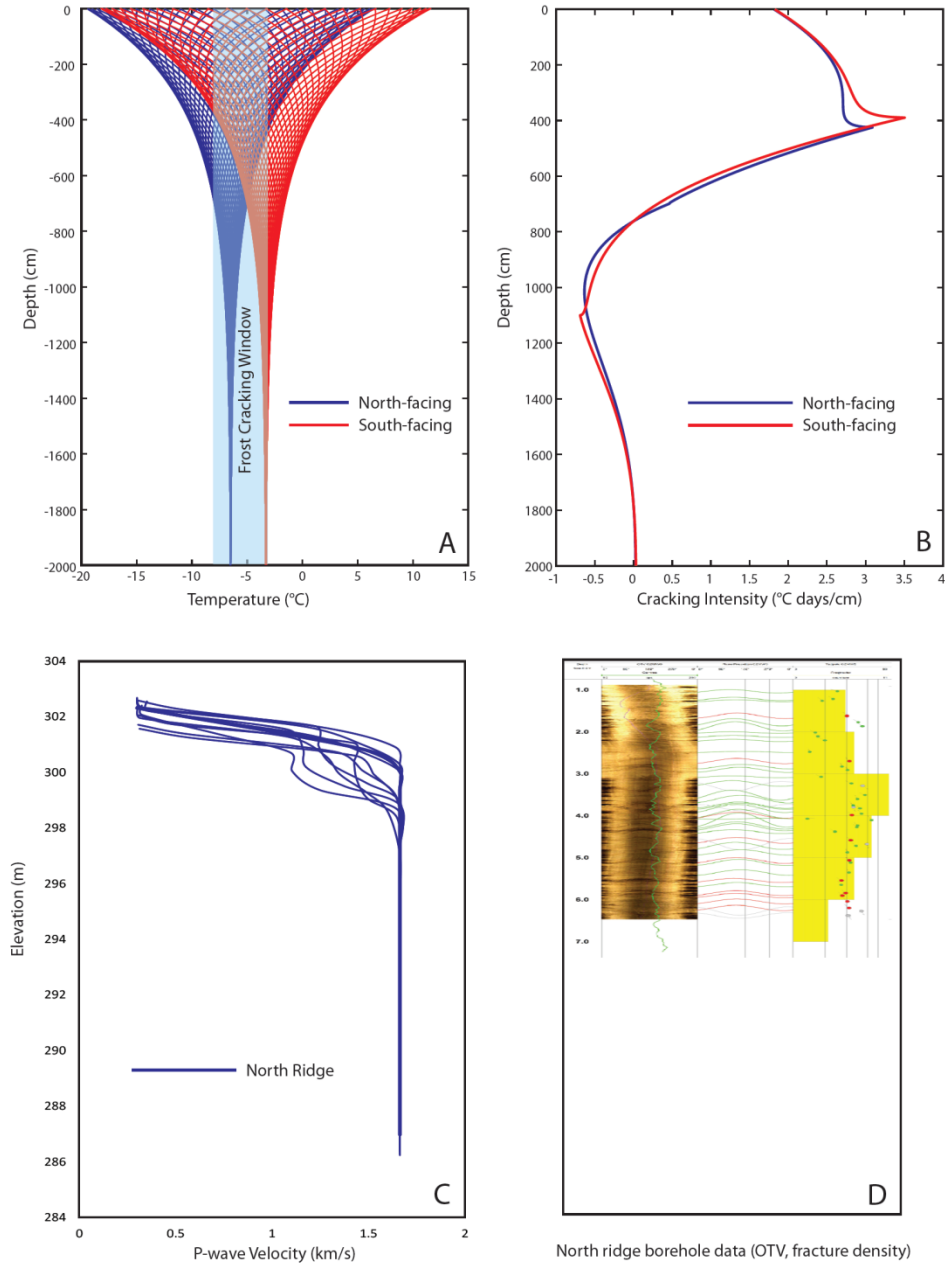


## Noteworthy Nuggets

The following figures and images have been submitted by the CZO team to show visually compelling progress.

H1.



Thermal diffusion model of assumed Pleistocene temperature conditions of N- and S- facing slopes MAT  $-6^{\circ}\text{C}$ ,  $-3^{\circ}\text{C}$ , respectively with thermal amplitudes of  $13^{\circ}\text{C}$  (A) produce frost cracking intensities that peak at 4m depth below ground surface (B). P-wave velocities along the N- ridge at SSHO are low to 5 m (C).

Optical televiewer logs for borehole CZMW5, completed along the N-ridge, show peak fracture densities at 4 m depth, declining to zero at ~7 m depth (D). Observed fracture densities and seismic p-wave velocities at SSHO correspond with predicted frost cracking intensities during the Pleistocene.

H2. and H3.

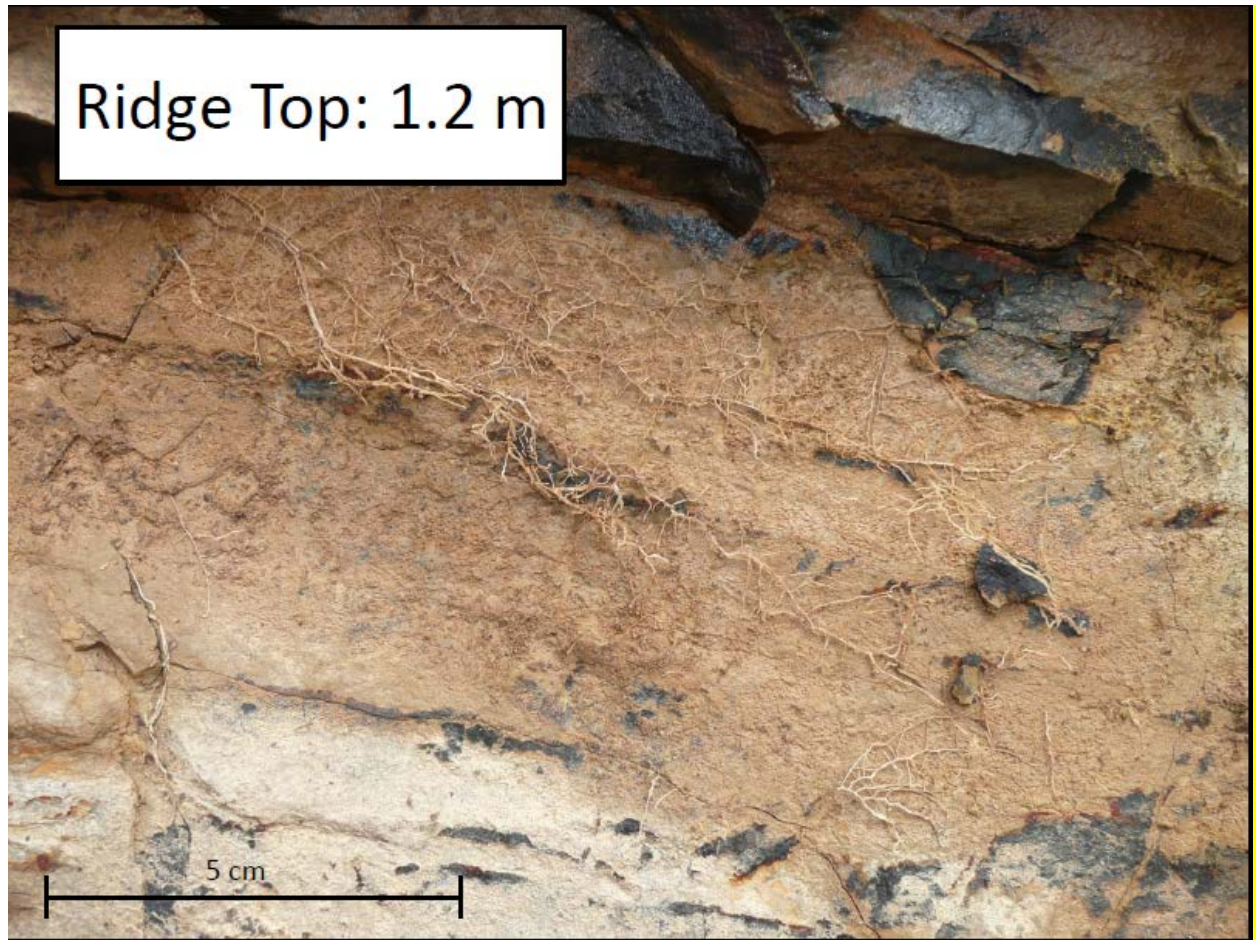
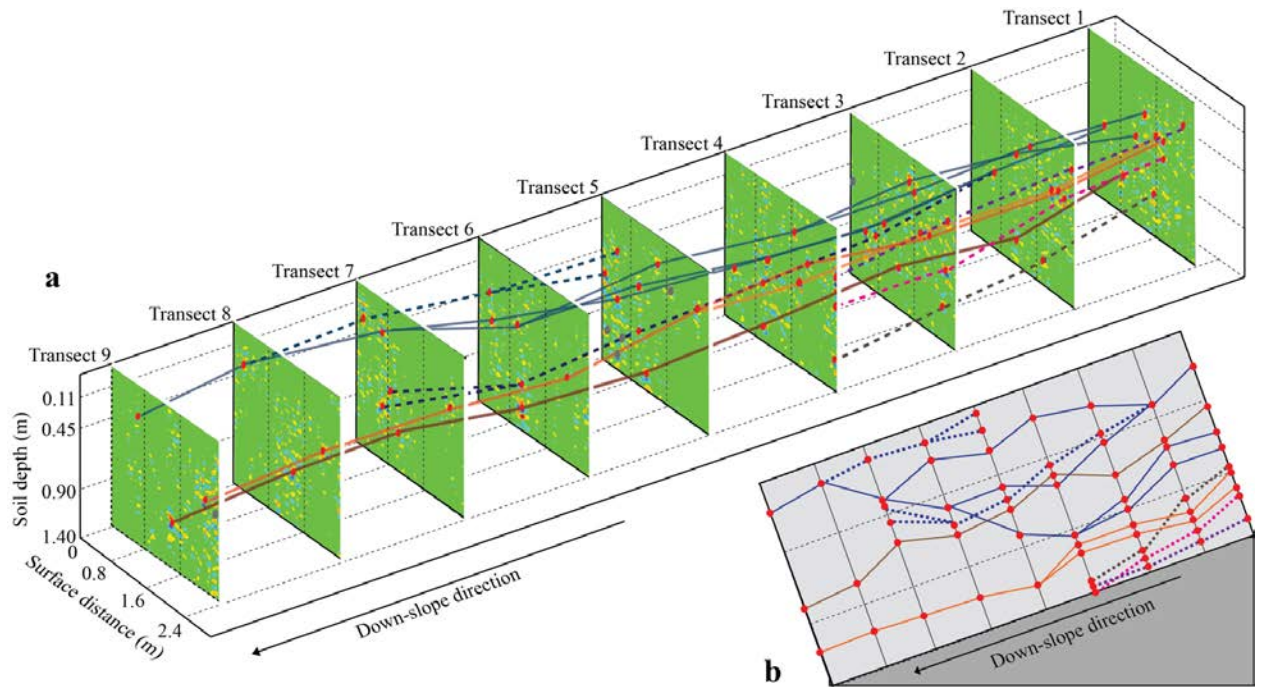


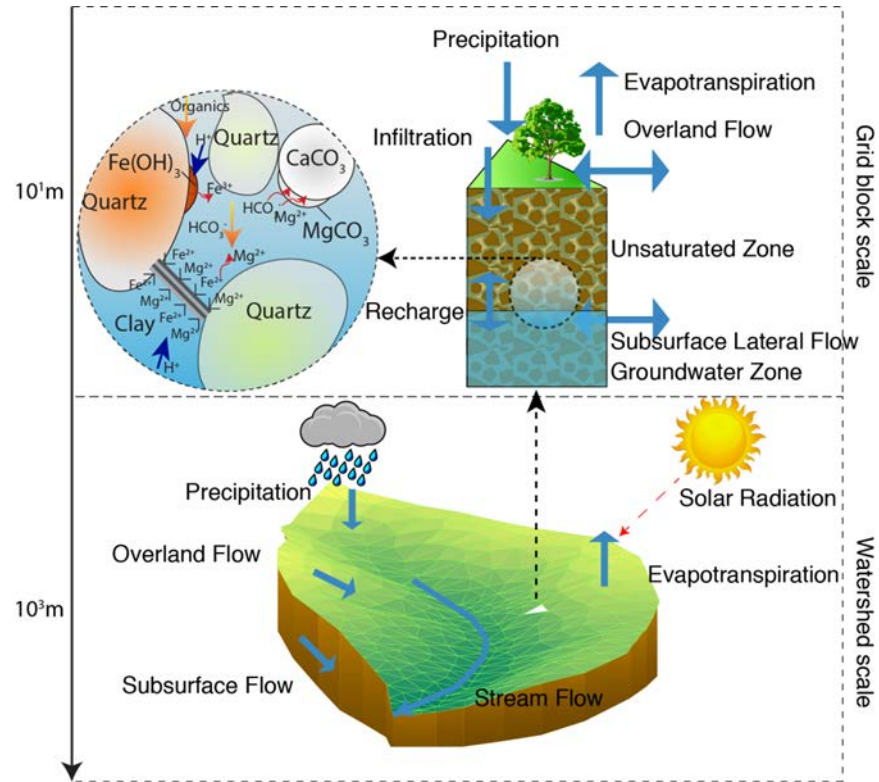
Image of roots growing in a fracture between two relatively unweathered shale fragments located a full meter below the bottom of the soil profile. It is yet unclear why roots grow this far below the soil, but their respiration rates are comparable to roots in surface soils. The rock around these roots have chemistry that is similar to parent material, and the thin layer of soil around the roots resembles B horizon material that was likely transported downward, rather than weathered in place.

H4.



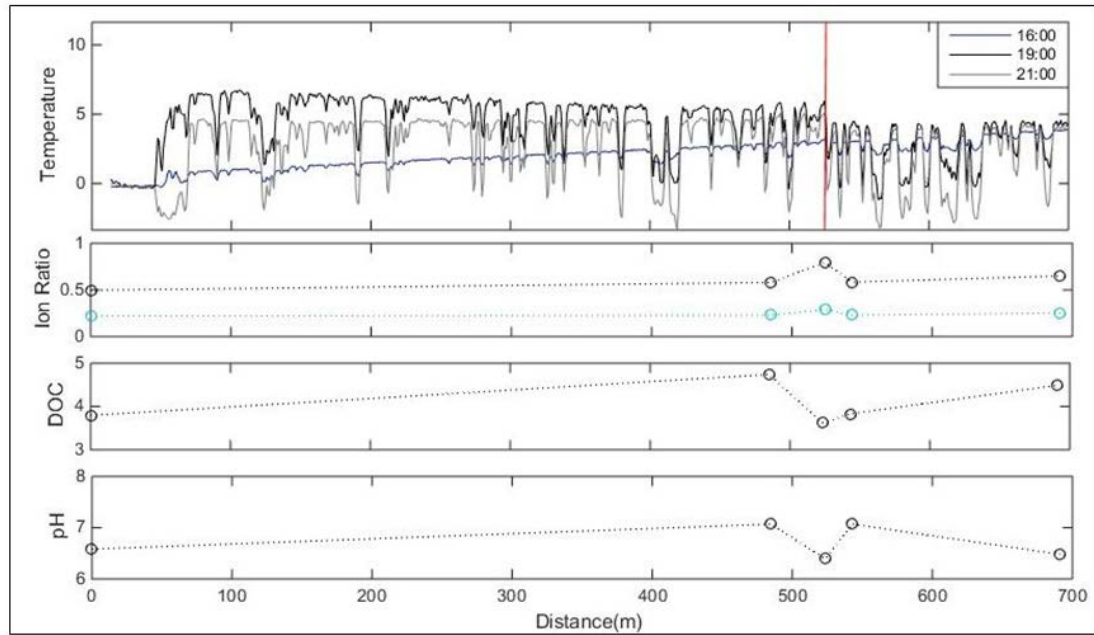
(a) Connection of corresponding subsurface lateral preferential flow (LPF) reflections on neighboring transects along the surveyed hillslope at Shale Hills to approximate a 3-D LPF network skeleton (based on the LPF identified). Red dots indicate the nodes of the LPF network on each subtracted GPR radargram, while gray dots (only a few, mainly in transect 5) indicate the LPF signatures that could not be connected between successive transects. (b) 2-D projection of the 3-D LPF network developed in (a) from the upslope transect 1 to the downslope transect 9. Dashed lines represent the LPF pathways that did not cross over the entire surveyed soil, while solid lines represent those LPF pathways that extended across all the survey transects. Different colors indicate different LPF pathways in both (a) and (b). Note that the scale of the downslope direction is intentionally exaggerated to provide a better visualization of the reconstructed LPF network.

H5.



Processes included in RT-Flux-PIHM. The coupled land surface hydrological model simulates the hydrological and land surface dynamics (precipitation, canopy interception, infiltration, recharge, overland flow, subsurface lateral flow, and surface energy balance) at the watershed scale using finite volume method. The model allows hydrological and biogeochemical coupling at the watershed scale. The discretized mesh structure for the Shale Hills Critical Zone Observatory is depicted at the bottom.

H6.



Four longitudinal profiles along Garner run in the new sandstone catchment: temperature, solute (ion) ratio, dissolved organic carbon (DOC), and pH versus distance along the stream. The temperature data (shown for three different time snapshots) were measured using the Distributed Temperature Sensor (DTS) from CTEMPS along the Garner Run study reach (700 m). The vertical red line indicates a location of groundwater input, inferred from DTS and stream chemistry data.

H7.

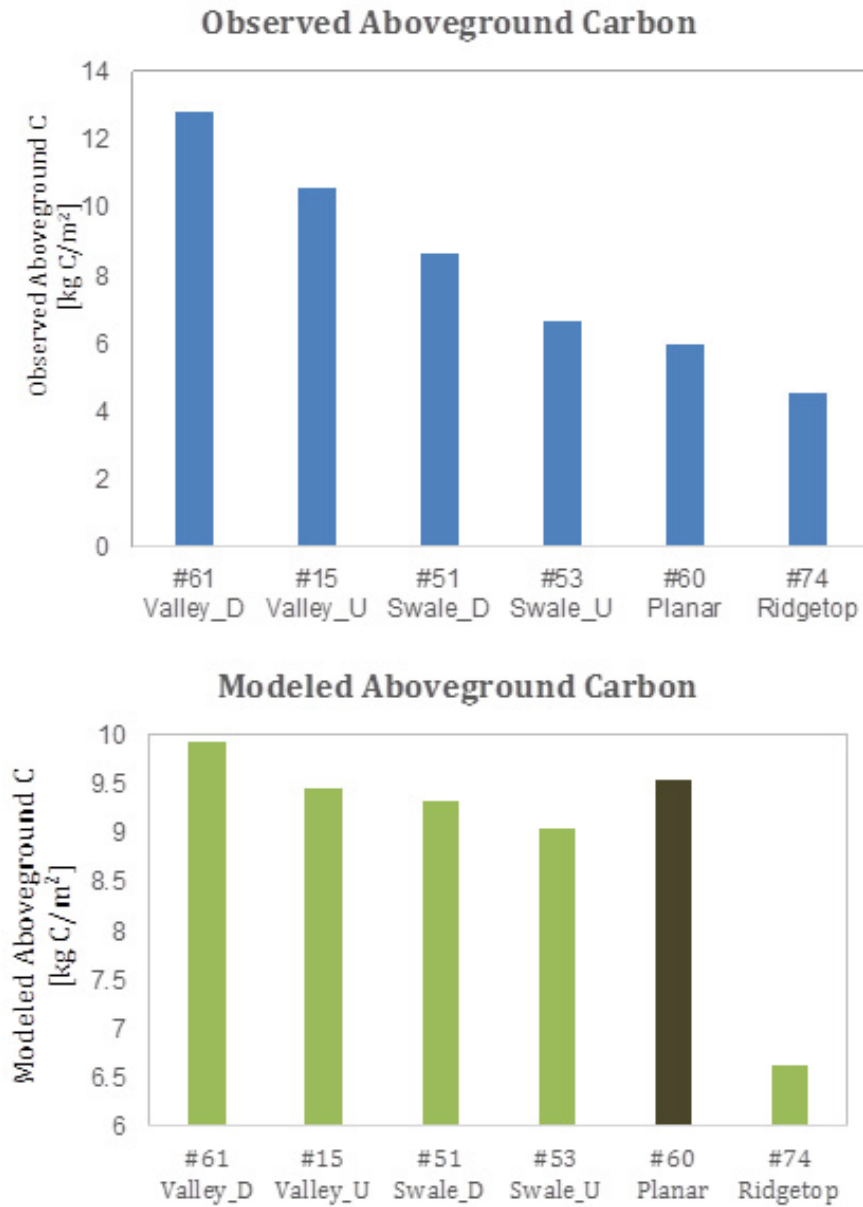
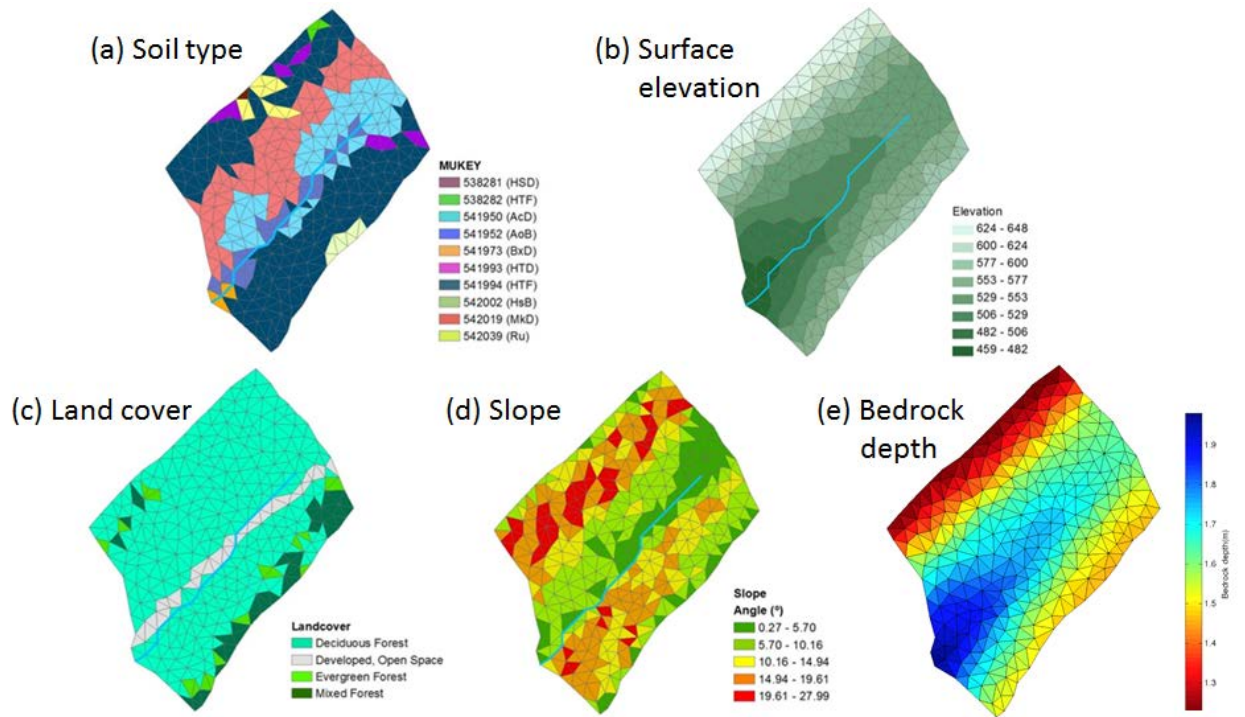
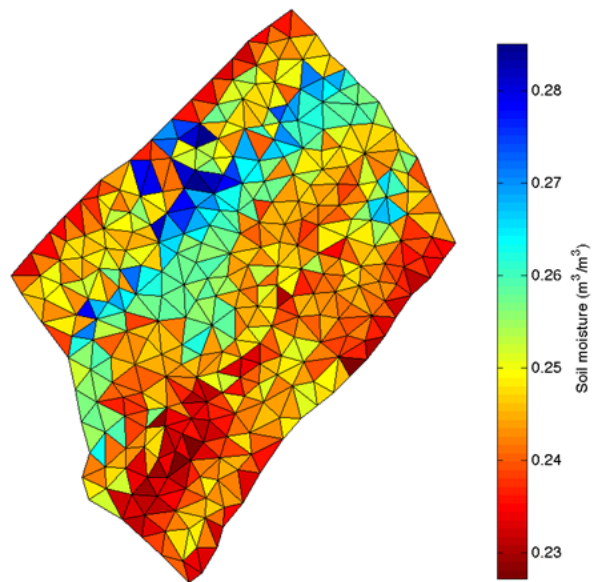


Figure shows the observed vs simulated above ground carbon stock as a function of position across the Shale Hills watershed. Differences in the simulation are driven by spatial variability in soil conditions, as imposed on the modeling system from point observations across the watershed. Site 60 is anomalously moist for its position in the watershed, leading to the relatively large modeled above ground biomass at that position.

H8.



Garner Run model domain set up for PIHM and Flux-PIHM models.



Flux-PIHM simulated annual average soil moisture (top 10 cm) pattern of 2009 at Garner Run. Note that the model is not calibrated using any field measurements.

H9.

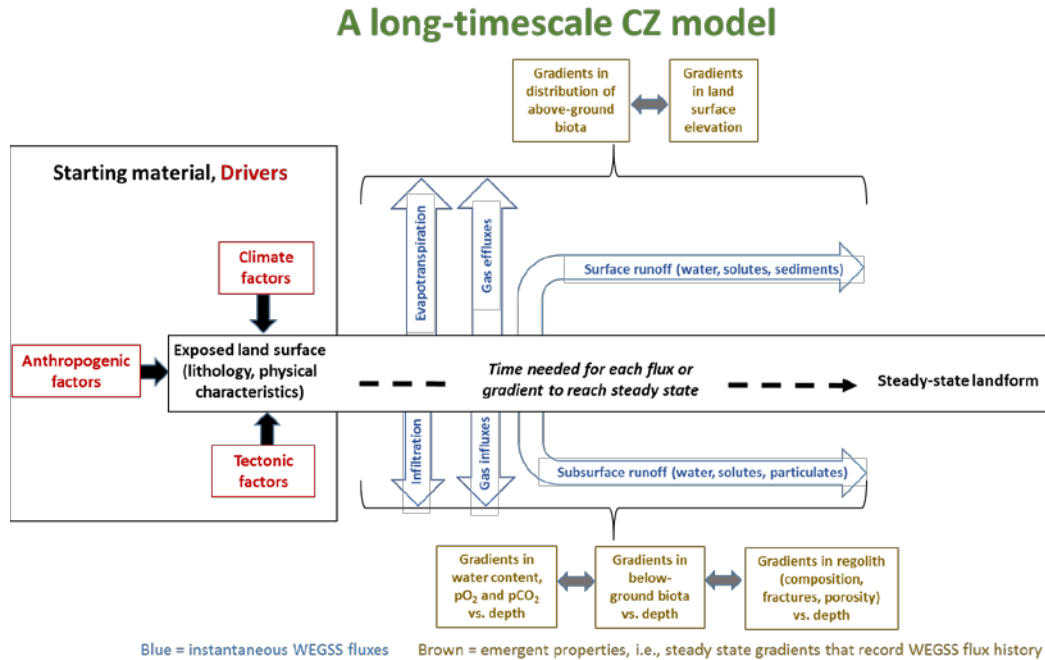
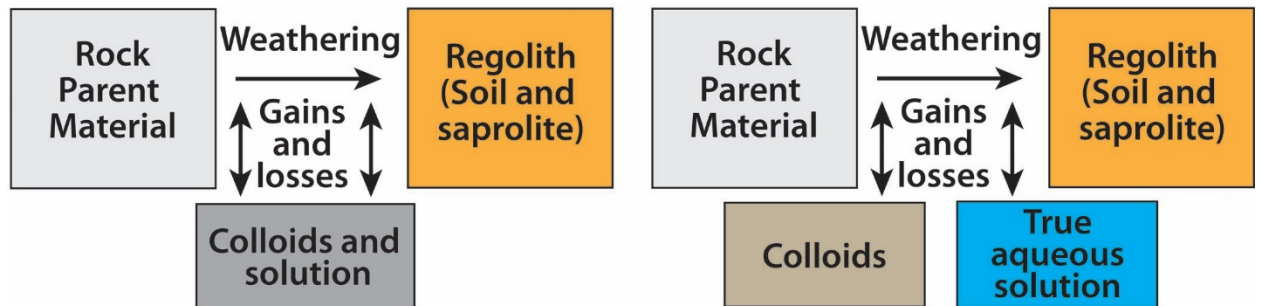


Figure documenting one picture of the long-term drivers and the resultant properties that emerge as part of the CZ. Each of these emergent properties can achieve a steady state after varying amounts of time: the emergent properties are lined up from left to right according to the increasing length of time needed to achieve steady state.

Seed Grant:



Open system mass balance of soils as carried out since 1897 (Merrill) and expanded upon by Brimhall and Dietrich (1987).

The dual-phase mass balance model (Bern et al., 2015) being applied to SSH and Luquillo CZO sites.

Figure depicting the additional process-level information to be gained about soil and CZ development from application of the newly developed dual-phase mass balance model (Seed grant PI: Carleton Bern, USGS).